Atmos. Chem. Phys., 26, 15877–15894, 2026
https://doi.org/10.5194/acp-26-15877-2026
© Author(s) 2026. This work is distributed under
the Creative Commons Attribution 4.0 License.

Atmospheric Chemistry and Physics
Open Access
EGU

Impact of aerosol absorption and scattering on winter fog lifecycle: insights from NWP simulations over Indo-Gangetic Plains

Shweta Bhati[1], Theethai-Jacob Anurose[1], Aravindakshan Jayakumar[1], Hamish Gordon[2], Anthony Jones[3], Saji Mohandas[1], and Vijapurapu Srinivasa Prasad[1]

[1]National Centre for Medium Range Weather Forecasting (NCMRWF), Ministry of Earth Sciences, Noida, India
[2]Department of Chemical Engineering and Center for Atmospheric Particle Studies, Carnegie Mellon University, Pittsburgh, Pennsylvania, USA
[3]Met Office, Exeter, United Kingdom

Correspondence: Shweta Bhati (shweta@ncmrwf.gov.in)

Received: 6 December 2025 – Discussion started: 3 February 2026
Revised: 27 August 2026 – Accepted: 10 October 2026 – Published: 11 November 2026

Abstract. The Indo-Gangetic Plains (IGP) of India frequently experience widespread and dense winter fog with substantial health and economic consequences. This season also coincides with elevated aerosol loading. This study investigates the influence of aerosols on the development and evolution of dense fog over the IGP using high-resolution numerical experiments. We focus especially on the relative contributions of absorption and scattering to aerosol-radiation interactions (ARI). While aerosol-cloud interactions related to fog have been extensively studied, the role of ARI has received relatively less attention, due to the limited prevalence of absorbing aerosols in many other parts of the world. However, the increasing number of absorbing aerosols over IGP prompted this study to isolate and examine the contributions of both scattering and absorbing components of ARI. Satellite-derived absorbing aerosol indices confirmed the presence of absorbing aerosols over the study region. The results of numerical experiments reveal that disabling the aerosol absorption component of ARI nearly doubled the area affected by dense fog, increased fog height by more than 20 %, and delayed fog dissipation by about 2 h. In contrast, turning off the scattering component of ARI reduced fog coverage by 18 %. Scattering effects were spatially uniform, promoting the vertical growth of fog. Conversely, absorption had a spatially variable impact, enhancing or suppressing fog height depending on whether the absorbing aerosols resided within or above the boundary layer. These findings emphasise the need to accurately represent ARI in numerical weather prediction models for improved fog forecasting over aerosol-rich regions like the IGP.

1 Introduction

Aerosols can directly scatter or absorb solar radiation, and together these processes constitute aerosol–radiation interactions (IPCC, 2013). Both scattering and absorbing aerosols perturb the energy budget by heating or cooling the atmosphere. It has been observed that in polluted environments, ARI cools the surface while warming the atmosphere aloft, enhancing atmospheric stability and suppressing boundary layer mixing, which favours the accumulation and formation of fine particulate matter during haze episodes (Wu et al., 2020; Yang et al., 2024). While scattering aerosols primarily contribute to the surface cooling by reflecting incoming solar radiation, absorbing aerosols – such as dust and black carbon (BC) – can warm the atmosphere by trapping radiation, thereby exerting a net warming effect on the climate (Sarkar and Panda, 2024). In addition to radiative effects, aerosols serve as cloud condensation nuclei (CCN), influencing cloud microphysical properties, including cloud lifetime, albedo, and precipitation processes. Although aerosol–cloud

interactions (ACI) are relatively well recognised, aerosol–fog interactions at meteorological scales remain less explored and poorly understood. This knowledge gap contributes to the challenges faced by current numerical weather prediction (NWP) models, which often struggle to accurately simulate fog events due to uncertainties in the representation of key processes governing fog formation, maintenance, and dissipation. ARI has been shown to play a critical role in modulating these processes (Sarin and Vinoj, 2026; Anurose et al., 2024; Li et al., 2022; Gautam et al., 2007).

In India, fog is a prominent meteorological phenomenon during the winter months of December, January, and February, often disrupting daily life and posing significant health and economic challenges (Ghude et al., 2017; Kulkarni et al., 2019). This is especially pronounced over Indo-Gangetic plains (IGP), a region that is not only a meteorological hotspot for dense fog but also one of the most polluted atmospheric zones in the country (Devi et al., 2020). Geographically, the IGP spans from 73° E, 32° N to 89° E, 21° N, encompassing diverse agro-climatic regions (Ali and Kumar, 2016). It houses several of India's most populous cities, including the National Capital Territory of Delhi – one of the largest urban agglomerations globally by population (World Population Review, 2024). The IGP frequently experiences widespread fog, primarily governed by high relative humidity and elevated aerosol concentrations (Ojha et al., 2020). In addition to being heavily aerosol-laden, the region forms part of one of the largest fluvial plains in the world and contains highly fertile soils (Srivastava et al., 2015; Rai et al., 2019). Agricultural activities, particularly winter crop irrigation, contribute to elevated soil moisture and ambient humidity, further intensifying fog formation (Smith et al., 2024). Moreover, post-synoptic high-pressure systems associated with Western Disturbances often lead to temperature inversions and stagnant air masses, which, combined with the trough-like topography of the IGP, trap pollutants and moisture near the surface, creating favourable conditions for persistent dense fog (Kutty et al., 2020).

High aerosol loading in the IGP plays a crucial role in the growth, sustenance, and dissipation of fog through both ACI and ARI. Early observational studies (Das et al., 2008) in the IGP established that increasing aerosol optical depth, decreasing surface temperatures, and higher relative humidity collectively favour fog formation. While several previous studies have investigated aerosol impacts on fog, most have focused primarily on ACI, which are generally considered dominant in fog microphysics and evolution. Several studies have reported a strong positive influence of ACI on fog lifecycle (Maalick et al., 2016; Boutle et al., 2018; Yan et al., 2021; Bharali et al., 2024).

In comparison, the role of ARI has received relatively less attention. However, the IGP is characterized by high aerosol loading during winter, including significant concentrations of absorbing aerosols such as black carbon and brown carbon arising from fossil-fuel combustion, biomass burning, and crop-residue burning. However, recent observations indicate a rising trend in absorbing aerosols across the region (Thomas et al., 2019; Ramachandran and Rupakheti, 2022). The impact of these aerosols is evident in both urban and rural settings: Gautam and Singh (2018) demonstrated the presence of "fog holes" over urban centres, likely driven by the urban heat island effect, while Anurose et al. (2024) reported similar fog-clearing patterns over rural areas attributed to radiative heating by absorbing aerosols through ARI. Therefore, the ARI effect, particularly its absorbing component, cannot be neglected over the IGP. These findings collectively highlight that aerosols significantly modulate fog processes in the IGP, both directly (ARI) and indirectly (ACI), making the region a natural laboratory for investigating aerosol effects on fog dynamics.

The IGP region has both industrial centres as well as densely populated cities with high vehicular traffic. The region remains a hotspot of black carbon, though some studies report a decreasing trend (Abdullah et al., 2025; Mehrotra et al., 2024). In addition to this, several studies have also reported significant brown-carbon absorption over the IGP, especially during winter, foggy episodes, biomass/crop-residue burning periods, and regional outflow events (Choudhary et al., 2024; Navinya et al., 2025; Shamjad et al., 2015). The influence of absorbing aerosols on fog or the relative contributions of aerosol absorption and scattering to fog evolution have not been examined in modeling studies over the IGP. Hence, it becomes important not only to study the role of ARI in fog lifecycle but also to examine the relative contributions of aerosol absorption and scattering in a polluted region like the IGP to fog responses.

With this background, the present study is aimed at understanding the influence of aerosols, particularly ARI, on fog over IGP using numerical modelling with a focus on dense fog conditions. The experiments have been designed to isolate the absorbing and scattering components of ARI within the same modelling framework, thereby allowing their relative roles in the temporal evolution, spatial extent, and vertical development of fog to be assessed. The findings may help provide a more process-level understanding of how different radiative properties of aerosols modulate fog evolution in IGP-like environments. Such understanding can support better-informed decision-making to regulate particulate matter pollution and mitigate the associated social and environmental impacts of dense fog.

2 Methodology and Data

2.1 DM-Chem Model Description

The NWP model employed in the present study is the Delhi Model with Chemistry and aerosol framework (DM-Chem1.0), which is a high-resolution (330 m) model used for operational forecasting of wintertime visibility and air quality at the National Centre for Medium-Range Weather Fore-

casting (NCMRWF), India. DM-Chem is a regional nested configuration of the Met Office Unified Model (Jayakumar et al., 2025), developed with a principal aim of forecasting visibility in fog. The modelling framework integrates the Delhi Model (DM) introduced by Jayakumar et al. (2018) with the UK Chemistry and Aerosol (UKCA) submodel (Gordon et al., 2018, 2023; Mulcahy et al., 2020). The initial version of DM-Chem is described by Jayakumar et al. (2021). The system was later enhanced and upgraded to version DM-Chem1.0 with improvements in model physics (Jayakumar et al., 2025; Mohandas et al., 2025). Key aspects of the model configuration and science details are summarised in Table 1, with detailed description available in earlier studies (Jayakumar et al., 2018, 2021, 2025).

2.2 Design of the Experiments

Fog over the IGP is most prominent during December-January, with persistent widespread episodes typically beginning in mid-December and extending into January (Singh and Gautam, 2022; Deshpande et al., 2023; Ghude et al., 2023). In the present study, simulations were carried out for the period of 1–10 January 2023, which experienced frequent occurrences of shallow to dense fog events almost daily (IMD, 2023). The DM-Chem model was run for a forecast length of 48 h based on 00:00 UTC initial conditions for each day. Subsequently, forecast outputs from $T + 12$ to $T + 35$ h were considered for analysis from each simulation. A series of experiments was designed to primarily investigate the impact of ARI on fog formation and evolution. First, a control simulation was performed using the operational version of DM-Chem1.0 (*Control*). Subsequently, before examining the impact of ARI, a simulation was conducted to assess the influence of aerosol concentration on fog evolution (*Aerosol Impact, AI*). For this purpose, input emissions of key aerosols and aerosol precursors (sulphate, organic matter, black carbon, H_2O_2, DMS, SO_2, DMSO, monoterpene, sea salt), were reduced by a factor of 10^3 to mimic near-pristine conditions (Yan et al., 2021). The resulting near-surface $PM_{2.5}$ concentrations remained below 5 µg m^{-3}, confirming a clean environment. Next, three sensitivity experiments were devised to isolate the effects of aerosol radiative properties. In these runs, aerosol absorption, scattering, and both absorption and scattering were sequentially disabled in the model. The sensitivity experiments were implemented within the UKCA aerosol–radiation coupling by directly modifying the aerosol optical properties supplied to the radiation scheme. For example, in the *ARII-A* experiment, the aerosol absorption coefficient was set to zero for all aerosol modes, atmospheric layers, and spectral bands, thereby suppressing the radiative effect of aerosol absorption while retaining the calculated scattering properties. This modification applies only to aerosol absorption and radiative absorption by atmospheric gases and clouds represented in the radiation scheme remains unchanged. Similarly, in the *ARII-S* experiment, the aerosol scattering coefficient was set to zero while retaining aerosol absorption, whereas both aerosol absorption and scattering coefficients were set to zero in the *ARII* experiment. The summary of all five experiments is provided in Table 2. The simulations were carried out for the outer domain of the DM-Chem1.0 setup (Table 1), which includes most of the IGP region. Some elevated regions within the domain (with surface altitudes above 450 m) were excluded from domain-wide analyses to minimise the influence of terrain-controlled fog processes.

2.3 Observational Data

The performance of the DM-Chem1.0 model for visibility was evaluated against observations from the weather station at Indira Gandhi International Airport (IGI), Delhi. Liquid water path (LWP) and single scattering albedo (SSA) were derived from the data products of the MODIS-Terra satellite. LWP was obtained from the MOD06_L2 cloud product (Platnick et al., 2015), while SSA is available as a standard retrieval within the MOD04_L2 aerosol product, where it is estimated using the Deep Blue algorithm (Levy et al., 2015). MODIS Terra passes over the study area at approximately 10:30 Indian Standard Time (IST; UTC+05:30). SSA products from MODIS were derived via post-processing using the Deep Blue algorithm. Further, SSA derived from in-situ observations of a few stations of the Aerosol Robotic Network (AERONET; Holben et al., 1998) were also utilized for model validation.

3 Results and Discussions

3.1 Model performance for visibility

Before delving into a detailed study of ARI using DM-Chem, the model's performance during dense fog conditions is evaluated in this section. Notably, DM-Chem has been actively used for fog-related research and for providing operational guidance over the IGP since 2018 (Jayakumar et al., 2025; Anurose et al., 2024). Further, the Unified Model has been used to study fog at high spatial grid resolution for many years, both without (Wilkinson et al., 2013; Boutle et al., 2018) and with (Ghosh et al., 2025) aerosol from UKCA and CASIM microphysics. Figure 1 displays the daily minimum visibility (Fig. 1a) and diurnal visibility patterns (Fig. 1b) during the study period from 1–10 January 2023. Fog classification is based on the India Meteorological Department (IMD) criteria: shallow fog is defined as a visibility of 501–1000 m, moderate fog as 201–500 m, and dense fog as 200 m or less (Jenamani, 2012). DM-Chem1.0 demonstrates good skill in reproducing the correct fog category for most days. In terms of diurnal evolution, the model realistically captures fog development during key hours – particularly between 00:00 and 09:00 IST – coinciding with observed and dense fog events. A bias in daytime visibility is

Table 1. Salient Features of DM-Chem1.0.

Details	DM-Chem1.0
No. of Domains	2 Outer: 500 × 500 grid points, resolution 1.5 km Inner: 300 × 300 grid points, resolution 330 m
Domain Extent	Outer: 25.16–32.15° N, 73.61–80.6° E Inner: 28.2–29.1° N, 76.65–77.55° E
Vertical Levels	70 vertical levels, with the first level positioned at 5 m above the ground and the top of the atmosphere set at 40 km
Cloud Microphysics	Double moment CASIM microphysics scheme (Field et al., 2023)
Cloud fraction Scheme	Bimodal cloud scheme (van Weverberg et al., 2021)
Urban parameterization	Detailed urban scheme, MORUSES with local morphology (Theethai-Jacob et al., 2023)
Irrigation representation	Irrigation is based on the irrigation scheme from the JULES land surface model. Soil moisture is always saturated over irrigated grasslands.
Aerosol Scheme	Two-moment GLOMAP-mode (Mann et al., 2010)
Dry deposition treatment	Meteorological dependent Wesely-type scheme (Wesely, 1989), considered for all the land surface categories.
Initialisation and boundary conditions	Meteorological and chemistry/aerosol initial and boundary conditions using NCMRWF operational setup outlined in Jayakumar et al. (2021)
Emission	EDGAR and SAFAR inventory for 1.5 km and 330 m domain, respectively.
Visibility parameterization	Number concentration from the coarse mode is additionally included apart from approach used in DM-Chem_baseline.

Table 2. Design of Simulations.

Experiment Name	Feature	Objective
Control	Simulation with operational DM-Chem1.0	Control Experiment
Aerosol Impact (AI)	Highly reduced emissions to represent a clean environment with minimal background particulate levels [$PM_{2.5} < 5\,\mu g\,m^{-3}$]	to study the impact of the presence of aerosols on fog
Aerosol Radiation Impact w.r.t. Absorption (ARII-A)	Aerosol absorption switched off in the Control setup	to study the influence of aerosol absorption
Aerosol Radiation Impact w.r.t. Scattering (ARII-S)	Aerosol scattering switched off in the Control setup	to study the influence of aerosol scattering
Aerosol Radiation Interaction Impact (ARII)	Both absorption and scattering by aerosols turned off	to study the influence of ARI

w.r.t.: with respect to

noted, likely due to the model underestimating particulate matter during daylight hours (Jayakumar et al., 2025). Nevertheless, the model accurately distinguishes between foggy and clear conditions. Subsequent analyses in this study emphasise dense fog-affected hours from 00:00 to 03:00 UTC (05:30–08:30 IST), during which the model has shown reliable performance. Further, comparison with the MODIS (Terra) satellite product for a dense fog day in the study period (7 January 2023) suggests that the model reasonably captures the spatial extent of fog, as reflected in the cloud liquid water path (LWP) distribution shown in Fig. A1 of the Appendix. A comprehensive evaluation of the model's performance for visibility and near-surface meteorological parameters is available in Jayakumar et al. (2025).

(a)

Fog Condition at Minimum Visibility		
Date	**Observed**	**DM-Chem1.0**
01-Jan-23	Dense Fog	Moderate Fog
02-Jan-23	Dense Fog	Dense Fog
03-Jan-23	Moderate Fog	Dense Fog
04-Jan-23	Dense Fog	Dense Fog
05-Jan-23	Dense Fog	Dense Fog
06-Jan-23	Dense Fog	Dense Fog
07-Jan-23	Dense Fog	Dense Fog
08-Jan-23	Dense Fog	Dense Fog
09-Jan-23	Dense Fog	Dense Fog
10-Jan-23	Dense Fog	Dense Fog

(b)

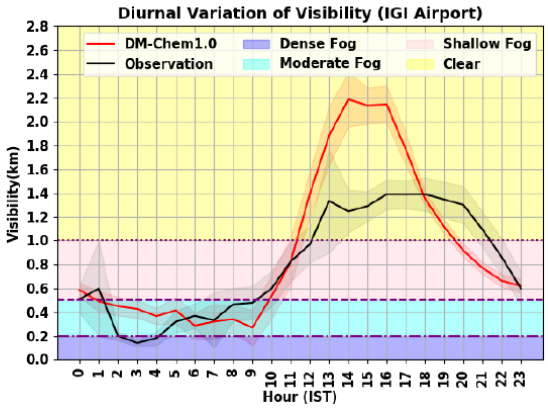


Figure 1. Comparison of observed and simulated visibility at IGI Airport for 1–10 January 2023 in terms of **(a)** daily minimum visibility within the 03:00–08:00 IST window, and **(b)** mean diurnal variation of visibility averaged over the 10 d study period, where solid lines denote the 10 d hourly mean for observations (black) and model (red), and shaded envelopes represent ±1 standard error across the days at each hour.

3.2 Aerosol absorption in the Indo-Gangetic Plains Region

As mentioned earlier, previous studies have reported increasing trends of absorbing aerosols in the IGP region (Thomas et al., 2019). The presence of absorbing aerosols in the study domain is examined in the present work using the Absorbing Aerosol Index (AAI) derived from the GOME-2/MetOp-C satellite instruments. The AAI is an index that indicates the presence of absorbing aerosols by comparing measured UV reflectance with simulated Rayleigh reflectance at 340 and 380 nm (Tilstra et al., 2010). Figure 2 shows mean AAI values for the study period (1–10 January 2023) as well as another time period (25–31 January 2023), which represents no-fog event days. As shown in Fig. 2, AAI values are predominantly positive across large parts of the model domain, indicating the widespread presence of absorbing aerosols. Further, Single Scattering Albedo (SSA) retrieved from two AERONET stations within the model domain are compared with that derived from DM-Chem1.0 at 440 nm as well as from the MODIS-Terra satellite in Fig. 3. SSA values are below 0.95, which are indicative of the presence of absorbing aerosols (Shin et al., 2019; Levy et al., 2010; Li et al, 2022). Additionally, SSA values retrieved from MODIS-Terra satellite data (Fig. A2) and other AERONET stations in the IGP region (Fig. A3) were also found to be below 0.95, further confirming the presence of aerosols with absorption characteristics in the region.

3.3 How do aerosols influence the spatio-temporal evolution of dense fog and how is this reflected in near surface parameters?

3.3.1 Aerosol-fog interaction: Insights into the role of ARI on the formation and evolution of dense fog

Aerosols impact both the thickness and lifetime of fog. Higher aerosol concentrations increase droplet numbers while reducing droplet sizes (Mazoyer et al., 2022), resulting in thicker fog layers. Figure 4 illustrates changes in the spatial extent of fog-affected areas across various experiments described in Sect. 2.2, relative to the *Control* experiment. Liquid Water Path (LWP) integrated over the first seven vertical levels of the model (~ 200 m) is used to characterise simulated fog. First, regions with LWP > 0 were used to identify fog-affected areas (Fig. 4, left panel). To specifically distinguish areas of dense fog, this condition was further refined by applying a visibility threshold < 200 m, combined with the condition LWP > 0 (Fig. 4, right panel). The influence of aerosol concentration on fog is most evident in the *AI* experiment, where areas with LWP > 0 decrease by about 78 % when particulate matter concentrations are reduced. Dense fog areas are nearly absent in this case. Temporal evolution of fog-affected areas, as a percentage of the total model domain, is presented in Fig. 5 from 18:00 to 17:00 (IST) the next day. The diurnal cycle is plotted from the evening hours of one day to the late afternoon of the following day so that the nighttime-to-morning period, during which visibility is generally lowest, and fog occurrence is highest, remains centred and continuous in the analysis. Areas with near-surface cloud liquid water mixing ratio (q_l) greater than 0.01 g kg^{-1} were marked as fog-affected areas (Maronga and Bosveld, 2017). The *AI* experiment shows the lowest fog coverage among all scenarios, with fog mostly confined to the nighttime hours

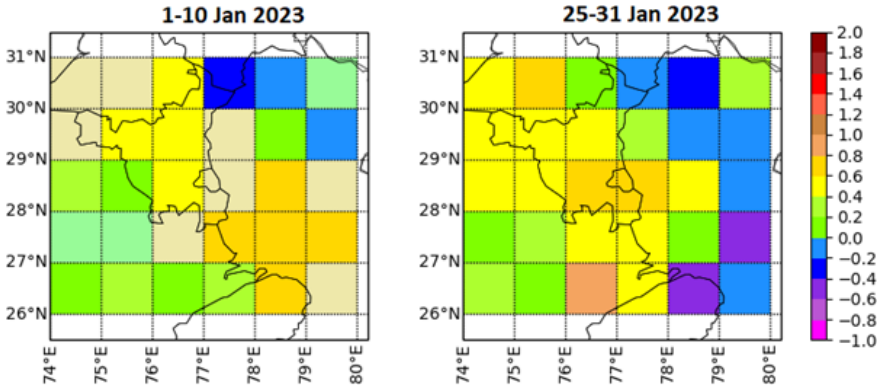


Figure 2. Mean Absorbing Aerosol Index in the Domain. Left: 1–10 January 2023, Right: 25–31 January 2023 (Clear days). Source: GOME-2/MetOp-C absorbing aerosol index.

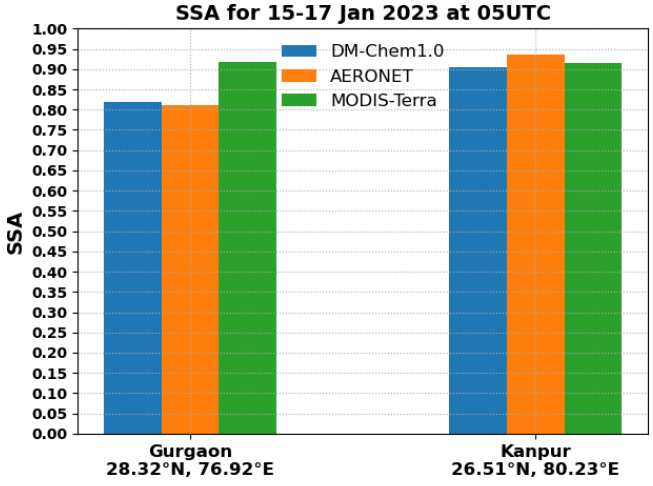


Figure 3. Mean Single Scattering Albedo (440 nm) at ∼ 05:00 UTC for two AERONET stations in the model domain for a no-fog period of 15–17 January 2023 [MODIS-Terra SSA at 470 nm].

(00:00–07:00 IST) – when low temperatures and high humidity still support fog formation, though not necessarily of dense character. After 07:00 IST, fog dissipates more rapidly as the highly reduced aerosol concentrations limit the efficiency of aerosol-driven microphysical processes, thereby weakening fog maintenance and growth.

Fog thickness is primarily influenced by its liquid water content and droplet size distribution. Aerosol absorption affects both by altering the microphysics – promoting droplet evaporation and suppressing droplet growth (Wagh et al., 2023; Boutle et al., 2018). As a result, thicker fogs with high optical depths may thin out when aerosols heat the fog layer and reduce droplet concentrations. In contrast, aerosol scattering favours fog formation by reducing the surface solar radiation, leading to cooler temperatures and enhanced radiative cooling. When aerosol absorption was eliminated from the model (*ARII-A* experiment), fog-affected areas increased significantly. Figure 4 (left panel) shows an increase in fog extent by around 48 %, while dense fog areas nearly doubled (Fig. 4, right panel) compared to the control experiment. In contrast, the *ARII-S* experiment (without aerosol scattering) showed a ∼ 18 % decrease in overall fog area and a 20 % reduction in dense fog regions. In the *ARII-A* experiment, fog coverage peaked at 36 % of the model domain at 08:00 IST, compared to 27 % in the *Control* experiment (Fig. 5). The maximum fog coverage in the *Control* experiment (27 %) was achieved 4 h earlier, around 04:00 IST in the *ARII-A* experiment, and fog persisted for about 2 h longer, indicating a delayed dissipation relative to the *Control*. Conversely, the *ARII-S* experiment peaked at just 23 %, further underscoring the crucial role of aerosol radiative properties in fog dynamics.

An increase in both the extent of fog areas and duration before complete dissipation, relative to the *Control* experiment, was observed in the *ARII* experiment. In this scenario, aerosols are present and can act as CCN, but they do not interact with radiation, neither through absorption nor scattering. Despite the absence of radiative effects, the presence of aerosols still promotes fog formation via microphysical processes. Notably, the fog behaviour in the *ARII* experiment more closely resembles that of the *ARII-A* experiment (where only absorption is disabled), suggesting that aerosol absorption has a stronger influence on fog lifecycle than scattering in this model domain. This highlights the role of absorbing aerosols in modulating ARI and their subsequent impact on fog characteristics.

Figure 6 shows the spatial distribution of ΔLWP, i.e., the change in LWP with respect to the *Control* experiment for the four experiments between 05:30 and 07:30 IST (00:00–02:00 UTC). The largest decrease in LWP was observed in the *AI* experiment primarily because of the absence of fog-sustaining aerosols. In contrast, a comparable increase in LWP was observed in the *ARII-A* experiment, where the lack of aerosol absorption enhances fog development and sustains higher LWP values.

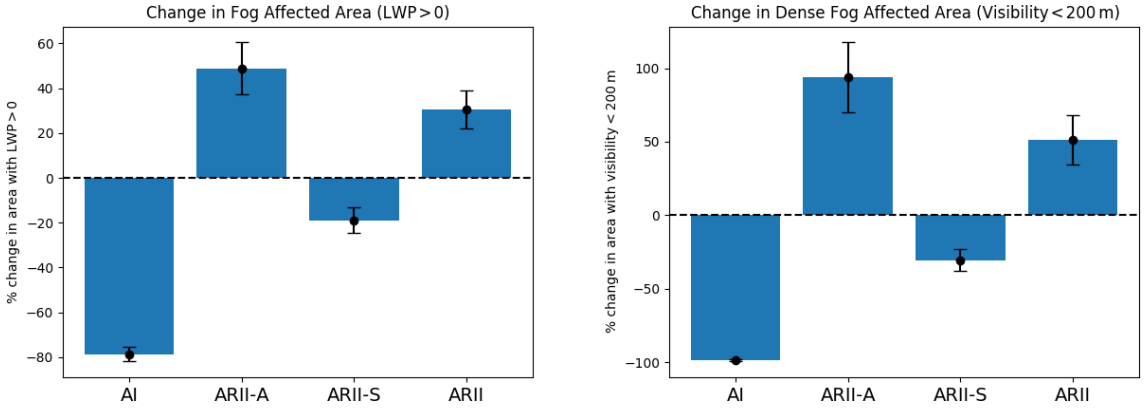


Figure 4. Change in Fog affected area with respect to control run in terms of (i) area with LWP > 0 (left), and (ii) area with visibility < 0.2 km (right).

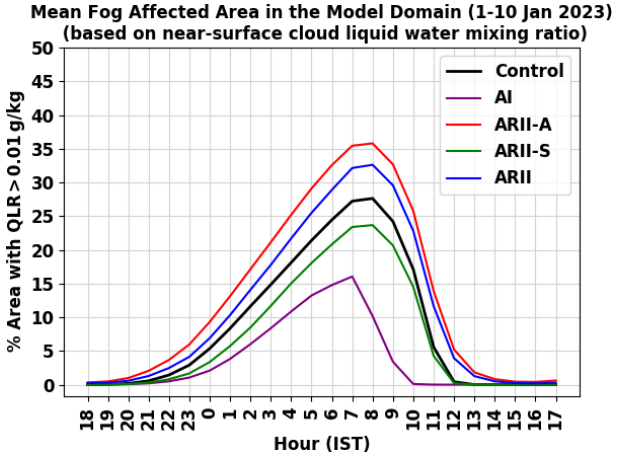


Figure 5. Diurnal variation of fog-affected area (% of total model domain) in different experiments.

3.3.2 Change in near-surface radiation fluxes and temperature

Figure 7 presents the mean diurnal variations in the differences in net longwave radiation (LWR; Fig. 7a), near-surface temperature (Fig. 7b), relative humidity (RH; Fig. 7c), and boundary layer height (BLH; Fig. 7d) across different experiments, each compared to the *Control* experiment. As shown in Fig. 5, the late afternoon to early evening period is largely fog-free across the model domain in all experiments. Since Fig. 7 is based on spatially averaged values over the entire domain, the 14:30–19:00 IST period is shaded in yellow to denote the hours when fog is absent in all experiments across the domain.

Among the surface radiation components, net longwave radiation dominates during winter, especially in January, when dense fog events commonly occur over the IGP, including the study region. Hence, as fog coverage starts to decline from 14:00 IST onwards, the differences in LWR among the various experiments also decrease, with minimal differences from 18:00–21:00 IST, reflecting a reduced role of fog and aerosol processes. At other, fog-prone hours, however, notable differences emerge. In the *ARII-A* experiment, an increase in downward LWR at the surface is observed. This can be attributed to the enhanced fog in this experiment, which contains more water droplets that absorb and re-emit longwave radiation, thereby increasing net downward LWR. A schematic for the radiation processes in the different experiments is displayed in Fig. 8. Under normal conditions, absorbing aerosols absorb incoming shortwave radiation, reducing the amount reaching the surface and causing ambient warming. This leads to atmospheric warming at the aerosol layer, while the surface may experience reduced shortwave heating. This warming limits the vertical growth at the time of fog formation and evolution. Hence, in the absence of aerosol absorption, the fog is denser and higher. Due to the presence of denser fog, which is highly effective at emitting downward longwave radiation (Li et al., 2021), an increase in net longwave radiation at the surface is exhibited in the *ARII-A* compared to the *Control* experiment.

In contrast, in the *ARII-S* experiment, fog is suppressed. Scattering aerosols reflect and scatter solar shortwave radiation back to space, leading to even stronger reductions in surface heating compared to absorbing aerosols. Therefore, in the *ARII-S* experiment, where scattering is absent, more solar radiation reaches the surface, causing stronger surface warming and, consequently, a greater increase in upwelling (outgoing) longwave radiation than in the *ARII-A* case. The reduced fog presence limits the re-emission of longwave radiation back to the surface, resulting in a decrease in net LWR compared to *Control*. In the *AI* experiment, where aerosols are entirely absent, the surface experiences strong direct heating due to uninhibited solar radiation. This leads to significantly enhanced outgoing longwave radiation, while downward LWR is minimal due to the lack of aerosols and fog.

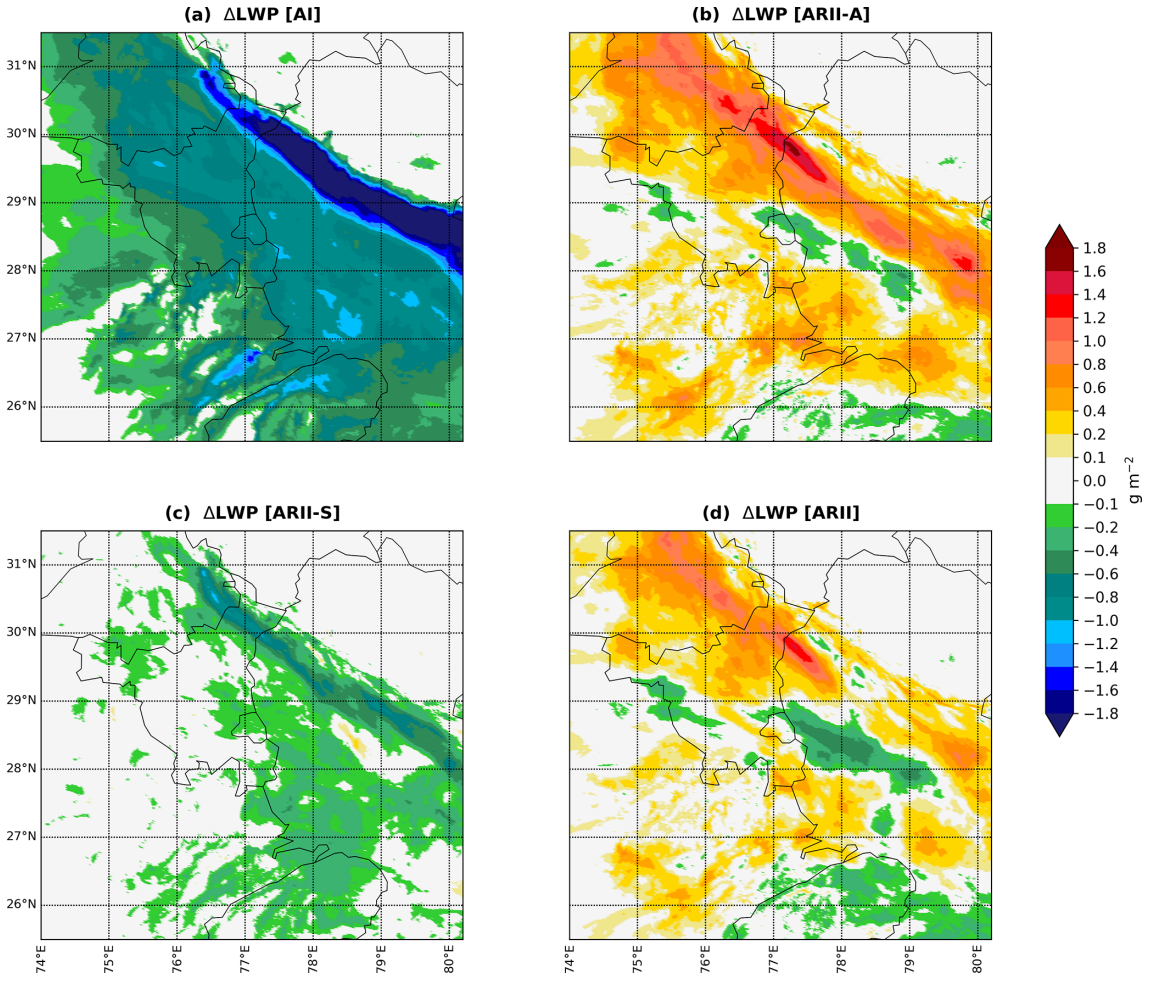


Figure 6. Spatial distribution of the mean difference in fog liquid water path (LWP g m^{-2}) [Experiment-Control] for 00:00–02:00 UTC (05:30–07:30 IST).

Consequently, the net LWR at the surface is substantially reduced.

The presence of enhanced fog in the *ARII-A* experiment leads to a decrease in near-surface temperature (Fig. 7b) and consequently an increase in relative humidity (Fig. 7c). The opposite effect is seen in the *ARII-S* experiment, where reduced scattering leads to increased near-surface temperature and reduced RH relative to the *Control* experiment. Notably, near-surface temperature, and consequently relative humidity, respond more directly to sunrise and sunset than net longwave radiation, which is indirectly modulated by changes in temperature, RH and fog. The sunrise-sunset transitions control the onset and cessation of shortwave (SW) radiative heating. As evening approaches, the shortwave pathway of aerosol-radiation interactions weakens and eventually becomes inactive, leading to a gradual reduction in temperature and relative humidity differences among the experiments. In the *AI* experiment, the virtual absence of aerosols and fog allows for greatly enhanced surface warming due to more incoming SW radiation. Consequently, most increase is observed in temperature (Fig. 7b), while relative humidity (RH) decreases (Fig. 7c). Even in non-fog hours, there is a difference of about 0.5 °C between the *Control* and *AI* experiments.

Boundary layer height (Fig. 7d) is closely linked to daytime temperature evolution. During nighttime and fog hours, BLH is higher in the *ARII-A* experiment. Normally, absorbing aerosols strengthen the inversion cap by stabilising the boundary layer and enhancing radiative cooling, which suppresses BLH development (Bharali et al., 2024; Su et al., 2020). In their absence, the inversion weakens, allowing BLH to increase. In contrast, scattering aerosols reduce radiative cooling at night. Their absence in the *ARII-S* experiment slightly decreases this suppression, leading to a modest increase in BLH. However, it is worth noting that aerosol scattering impacts longwave radiation to a lesser extent than shortwave, unless under conditions of heavy particulate pollution (Liu et al., 2024). As fog dissipates during the late morning and solar radiation intensifies into the afternoon hours, the BLH response changes. The elevated atmo-

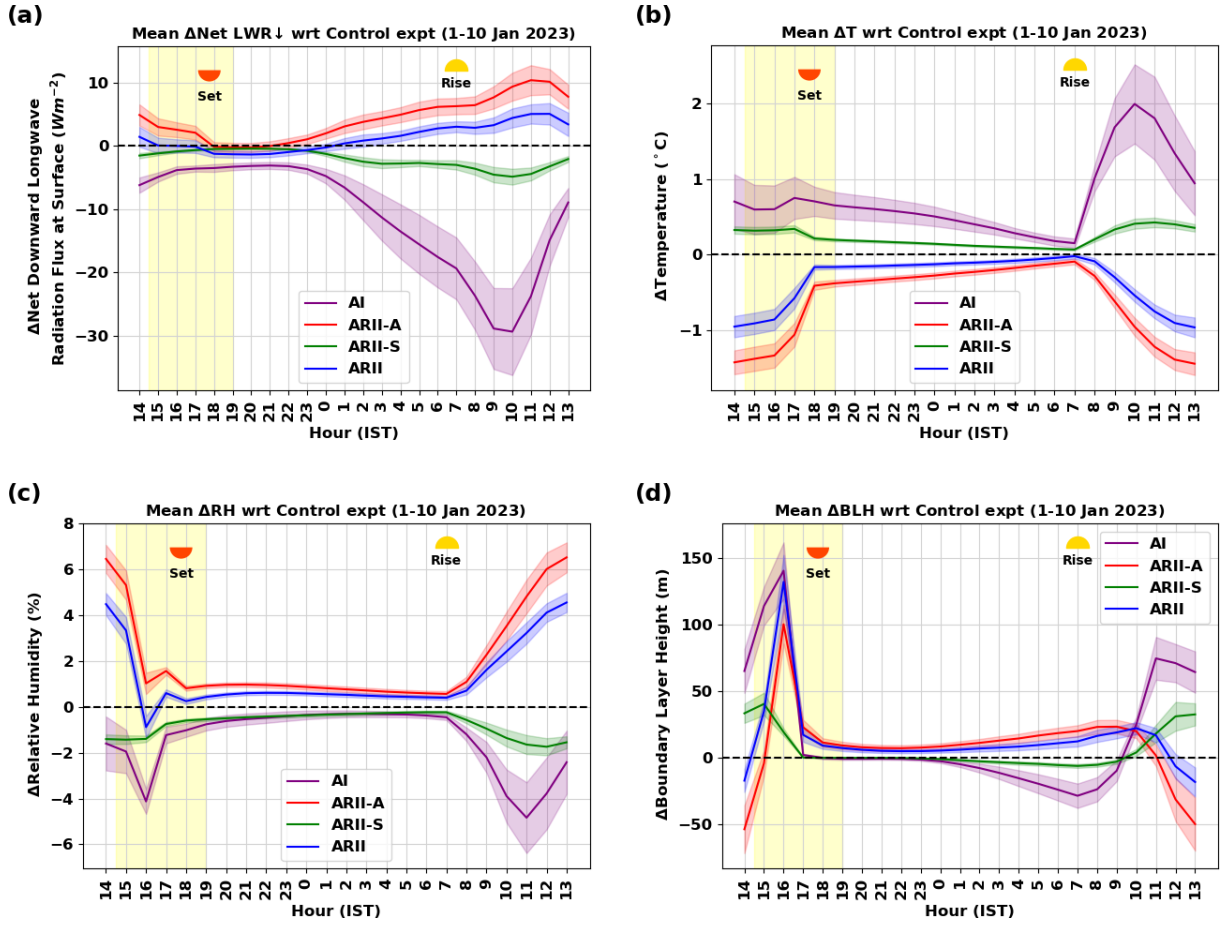


Figure 7. Diurnal variability of changes with respect to the *Control* experiment [Experiment-Control] (along with standard error) for **(a)** Net Surface Longwave Radiation, **(b)** near surface temperature, **(c)** relative humidity, and **(d)** boundary layer height. The yellow shading indicates the hours during which fog is absent in all experiments across the model domain. Approximate sunrise and sunset times during the study period are also marked in each panel.

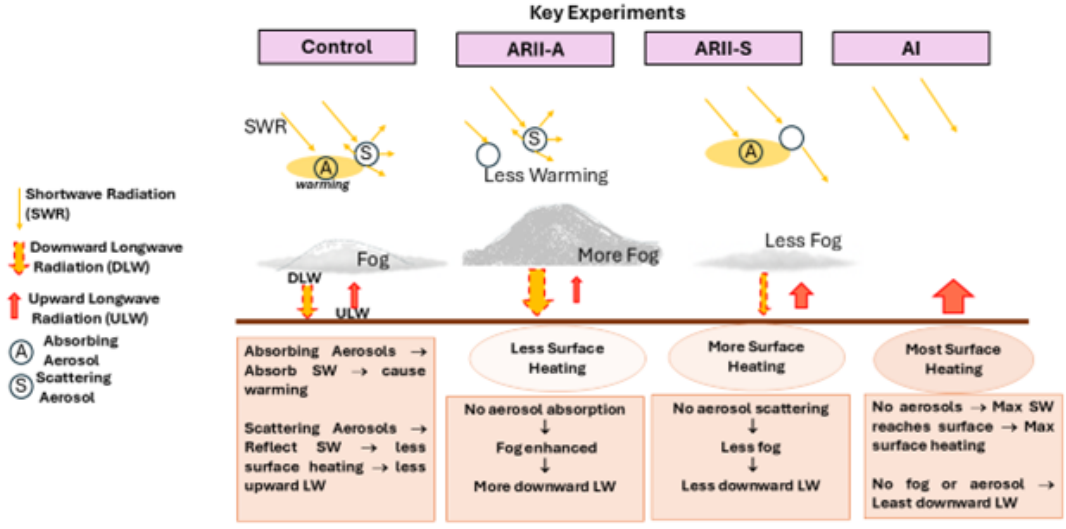


Figure 8. Schematic for key radiative processes in different experiments.

spheric heating fuels growth in BLH in the *Control* experiment. This absorption-driven heating is absent in the *ARII-A* experiment, while surface heating is enhanced in the *ARII-S* experiment. Consequently, the BLH difference turns negative from around 11:00 IST in *ARII-A* and positive in *ARII-S*. As we approach post-maxima afternoon hours (which are also fog free hours), there is a changing balance between weakened atmospheric heating and greater near-surface heating driven turbulence in the *ARII-A* experiment. The decline in BLH after reaching daytime maxima is more gradual in the *ARII-A* experiment, which leads to a sharp rise in the BLH difference between *ARII-A* and *Control* during this window (14:00–15:00 IST).

3.4 Influence of ARI on vertically resolved fog properties

Understanding how ARI influences the vertical evolution of fog is crucial for assessing its formation and persistence. Figure 9 presents the vertical cross-sections of the cloud liquid water mixing ratio (q_l), showing average hourly values across the entire model domain, with the vertical coordinate expressed as height above the local surface. In the *ARII-A* experiment (Fig. 9b), sufficient radiative cooling enables fog formation approximately an hour earlier ($\sim$ 23:00 IST) than in the *Control* experiment (Fig. 9a). Similarly, the fog dissipation near the surface is delayed by about an hour (Fig. 9b). In contrast, the *ARII-S* experiment has a weaker impact on fog onset and dissipation (Fig. 9c), with onset advancing by less than an hour and dissipation time changing negligibly compared to the *Control* experiment. Most prominent differences are observed in the vertical profile of q_l. Fog generally persists up to $\sim$ 240 m in the *Control* experiment. This height increases to $\sim$ 300 m in the *ARII-A* experiment and reduces to $\sim$ 210 m in *ARII-S*. These results align with the overall reduction in the radiative warming in the *ARII-A* experiment and enhanced surface heating in *ARII-S*. In the *AI* experiment (Fig. 9e), fog does not form at all, with q_l values remaining below the minimum fog threshold of 0.01 g kg^{-1} at the domain-wide average level. Thus, Fig. 9e is shown with a different q_l scale. This underscores the importance of ACI, wherein aerosols serve as CCN, facilitating fog growth. Overall, ACI has a stronger influence than ARI on the growth and evolution of dense fog, corroborated by previous findings (Yan et al., 2021). Nevertheless, the increase in fog height from $\sim$ 240 m in the *Control* experiment to about 300 m in the *ARII-A* experiment indicates that suppressing aerosol absorption can increase fog height by about 25 %. This highlights the non-negligible contribution of *ARI* alongside the dominant role of *ACI* during dense fog events over the IGP.

Figure 9 indicates that maximum fog height typically occurs between 08:00 and 10:00 (IST). To assess the spatial impact of various experiments on fog height, further analysis was carried out at 03:00 UTC (08:30 IST). The spatial distribution of differences in fog height across the domain at this time is presented in Fig. 10. As previously mentioned, regions with surface altitudes exceeding 450 m were excluded from the analysis. The *ARII-S* experiment generally reduces fog height, a trend also observed in the AI experiment, where suppression of fog height is widespread. Fog top height is reduced quite uniformly across the model domain in both *ARII-S* and *AI* experiments. In contrast, the *ARII-A* experiment shows a more heterogeneous response. While fog height increases across large portions of the domain, certain areas experience a decrease. This spatial variability is likely linked to the vertical distribution of absorbing aerosols.

A more detailed examination of such two contrasting regions (Figs. A4 and A5) reveals notable differences in the vertical aerosol profiles above and below the boundary layer. In the region exhibiting a negative fog height response to the *ARII-A* experiment, there is a higher concentration of absorbing aerosols (BC) near the surface, while concentrations above BLH are nearly an order of magnitude lower. This leads to a steep vertical gradient in aerosol distribution in fog-suppressing regions, with elevated near-surface levels. Such a profile suggests a dominant influence of surface heating, potentially overpowering the atmospheric warming aloft. Elevated concentrations of absorbing aerosols within the boundary layer can increase near-surface air temperatures, thereby raising the BLH (Bharali et al., 2024), which is the case in the *Control* experiment. Consequently, when aerosol absorption near the surface is suppressed in the *ARII-A* experiment, the boundary layer becomes shallower in such regions, which, in turn, reduces the fog top height. These findings highlight the complex interplay between aerosols and meteorological processes. The vertical placement of absorbing aerosols relative to the boundary layer critically influences fog dynamics, underscoring the need for further investigation into these coupled interactions.

4 Discussion and Conclusions

Widespread dense fog is a frequent and persistent phenomenon over the Indo-Gangetic Plains during the winter season. This region is also characterised by high aerosol loading, and several studies over the IGP have reported appreciable concentrations of absorbing aerosols. This makes it important to examine how aerosol-radiation interactions can influence the formation, persistence and dissipation of fog in the region. In this study, four targeted numerical experiments were conducted using the DM-Chem1.0 model to isolate the relative contributions of the absorbing and scattering components of ARI to fog characteristics in the IGP region during January 2023.

- When the absorbing effects of aerosols were suppressed in the *ARII-A* experiment, fog was found to be denser and more persistent, covering a larger horizontal area and extending through a greater vertical depth.

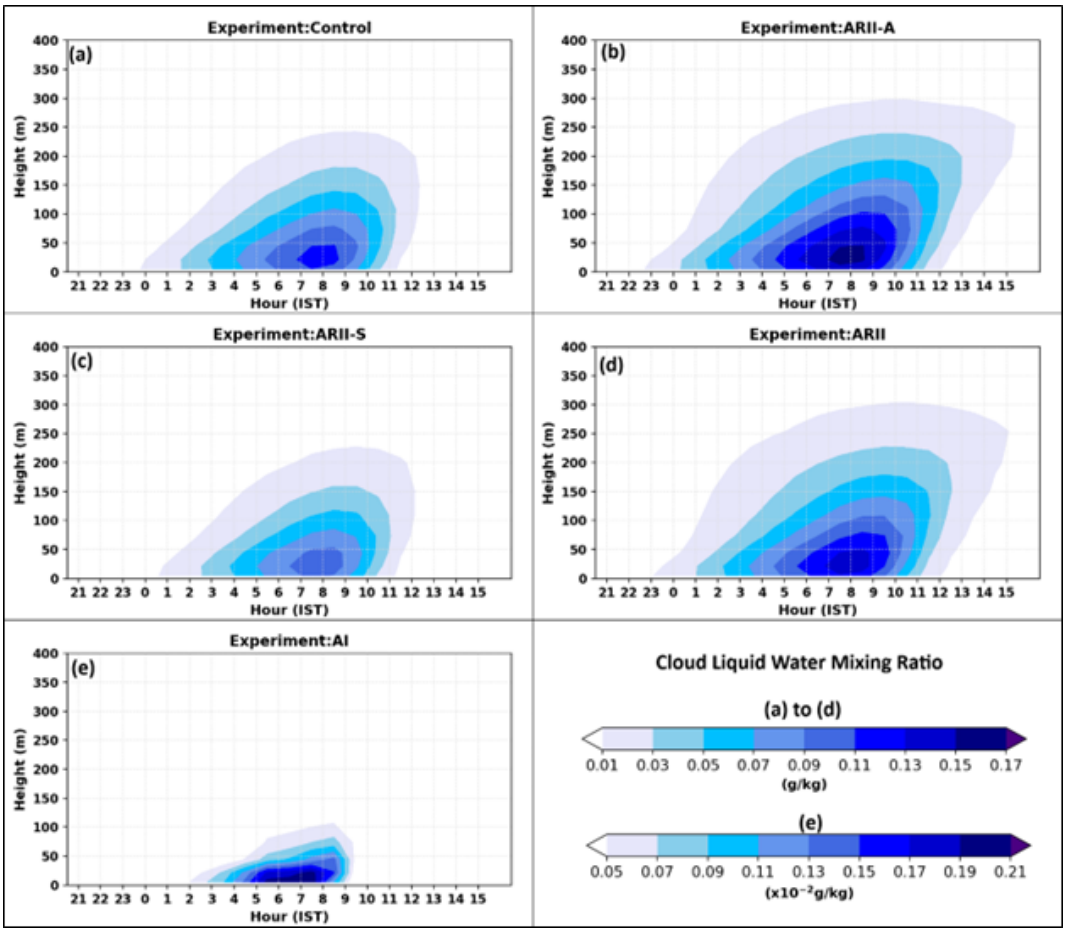


Figure 9. Vertical profile of (domain averaged) Cloud Liquid Water Mixing Ratio for 1–10 January 2023.

- In contrast, disabling the scattering of radiation by aerosols in the *ARII-S* experiment limited the vertical development and spatial extent of fog. However, the enhancement of fog characteristics observed in *ARII-A* was more pronounced than the reductions seen in *ARII-S*.

- When both absorption and scattering were deactivated in the *ARII* experiment, the resulting fog behaviour still resembled that of the *ARII-A* scenario more closely than *ARII-S*. This indicated a greater influence of absorbing aerosols in the IGP region.

- The *AI* experiment, which simulated a clean environment with minimal particulate matter, failed to achieve conditions conducive to fog formation over large parts of the study domain. It shows the lowest fog coverage, with fog mostly confined to nighttime hours, followed by the earliest and most rapid dissipation. This underscores the critical role of heavy aerosol loading in the IGP region, suggesting it is a dominant factor in initiating fog formation.

The major inference that can be drawn from the simulations conducted in this study is that while aerosol availability is crucial for initiating fog formation, the absorbing and scattering components of ARI significantly influence subsequent fog growth, maintenance, and dissipation. The findings in this study contrast with those of Yan et al. (2021), who reported that ARI has a negligible effect on fog lifetime in East China. However, some studies suggest that ARI plays an important role in heavily polluted environments. Ding et al. (2019) found that the effect of ACI was weaker than that of ARI on the formation and evolution of fog during a haze pollution episode in the Yangtze River Delta region in eastern China. This aligns with broader modelling evidence from Liu et al. (2020), who reported that ACIs tend to saturate at high aerosol loading, whereas the strength of ARIs continues to increase and plays a more important role in highly polluted episodes. Peng et al. (2022) also noted that ARI has a critical influence on the outbreak of severe haze-fog by virtue of reducing surface solar radiation, which further leads to weakened turbulence, reduced temperature, and increased humidity favouring hygroscopic growth of aerosols.

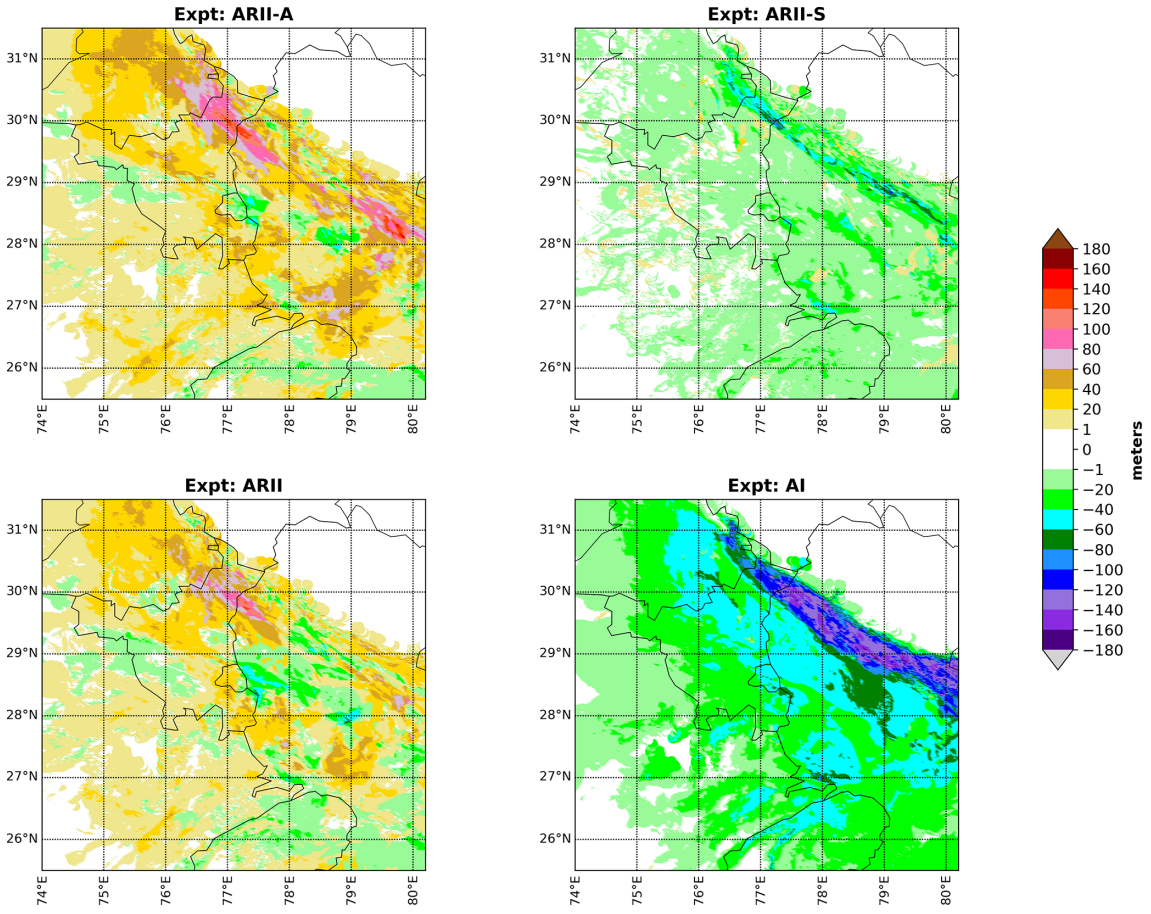


Figure 10. Difference in Fog Height with respect to the *Control* experiment at 03:00 UTC (08:30 IST).

Specifically, over the IGP region, Bharali et al. (2024) also drew a similar inference from their investigation of a dense fog episode that the aerosol–radiation feedback plays an important role in the intensity and lifetime of fog. Arun et al. (2025) used the WRF-Chem model to conduct a suite of experiments to assess the relative importance of ARI and ACI over the IGP region. They concluded that ACI is the dominant pathway in fog formation while ARI influences surface stagnation, cooling, and moistening, thereby affecting fog persistence and dissipation. In the present study, we further examined the relative roles of the absorbing and scattering components of ARI and found that aerosol absorption appears to play an important role in the study region, as also noted by Anurose et al. (2024). The AAI values, which indicate a considerable presence of absorbing aerosol types, support the aerosol environment represented in the model and lend credibility to experimental focus on aerosol absorption in the context of the IGP region.

The interpretations presented in this study, however, are primarily based on model simulations conducted for a single period in January 2023. Winter-time fog over the IGP is a regional phenomenon driven by favourable synoptic-scale influences such as western disturbances (Smith et al., 2023), land-surface moisture enhancement by irrigation practices (Smith et al., 2024), and competing influences from urban surfaces and urban aerosols (Anurose et al., 2024). These factors do not operate independently of the different ARI responses examined in the present study. All these factors can modify radiative cooling, surface energy balance, humidity, turbulence, and boundary-layer depth, thereby influencing overall fog lifecycle. Further, fog conditions significantly impact the applicability or reliability of both satellite aerosol retrievals and in-situ observations at several sites within the study region. This has restricted direct point-to-point validation in this study and highlights the importance of expanding and strengthening the observational network to enable more robust assessments. Nonetheless, the findings of the present study underscore the necessity of accurately representing the ARI processes in NWP models to improve fog forecasts. Additionally, further studies on aerosol size distribution and chemical composition are essential to enhance the representation of ARI in modelling systems.

Appendix A

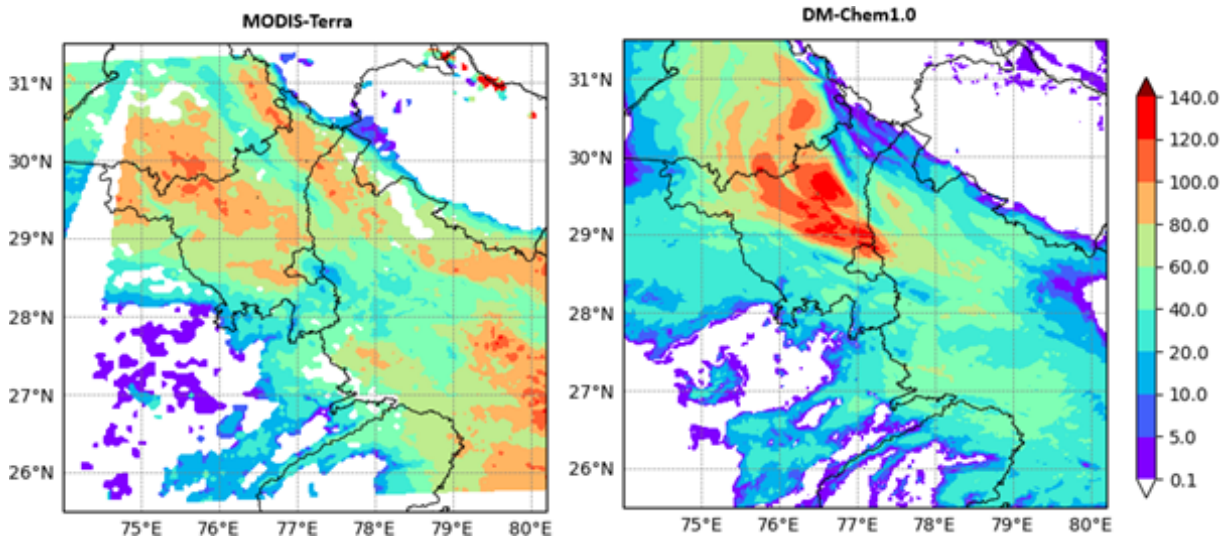


Figure A1. Cloud Liquid Water Path ($g\,m^{-2}$) for 7 January 2023 (dense fog day).

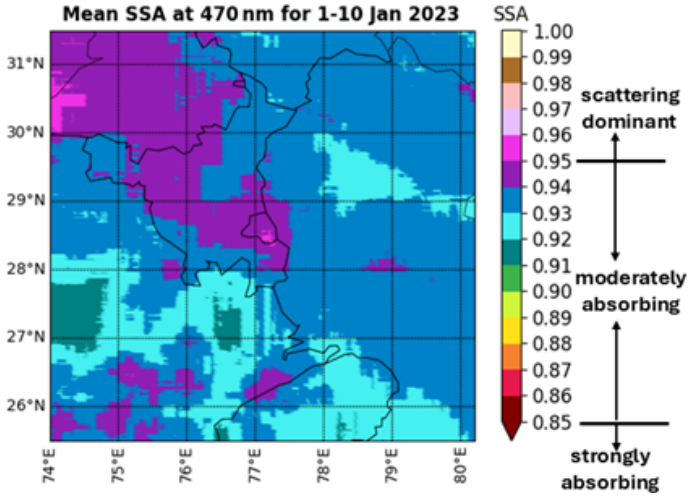


Figure A2. Mean Single Scattering Albedo over study region (1–10 January 2023) from MODIS.

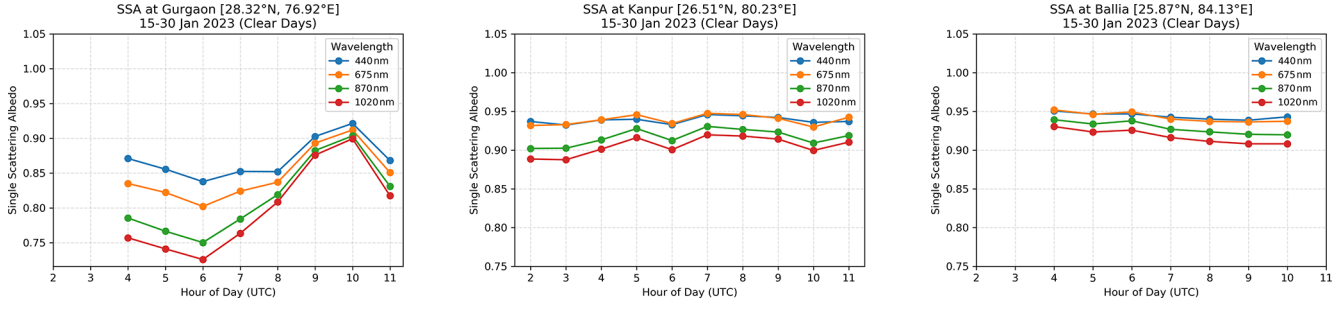


Figure A3. Mean Single Scattering Albedo as observed at AERONET stations within IGP during January 2023.

Many absorbing aerosols (e.g., black carbon from biomass burning and urban pollution) have their strongest absorption in the UV and blue spectral range. Figure A2 displays the single scattering albedo (SSA) derived from spectral SSA retrievals with MODIS at 470 nm, averaged over the study period. Most of the region demonstrates SSA values between 0.90 and 0.95, indicating a moderately absorbing character (Ramachandran et al., 2022). However, satellite aerosol retrievals are much more reliable under clear-sky (cloud-free) conditions. The period of 150-30 January 2023 had very few fog-affected days. Figure A3 shows SSA values observed at three AERONET stations within the IGP region for 15–30 January 2023 at different wavelengths. Most of the values are below 0.95. Additionally, decreasing values of SSA with increasing wavelength have been found to be indicative of aerosol mixtures containing absorbing aerosols, such as black carbon (Li et al., 2015). This signals an appreciable presence of absorbing aerosols in the IGP region.

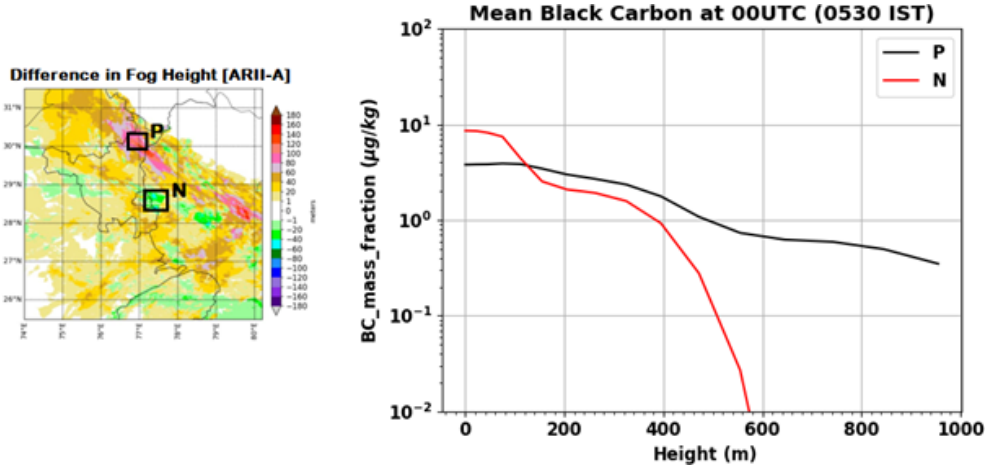


Figure A4. Simulated vertical distribution of mass mixing ratio of black carbon (right panel) for two regions exhibiting positive change [P] or increase in fog height and negative change [N] or decrease in fog height with absorption off (*ARII-A*) experiment (00:00 UTC) as seen in Fig. 10 (left panel). N region shows a sharp decline in BC levels above boundary layer height (BLH) compared to P region.

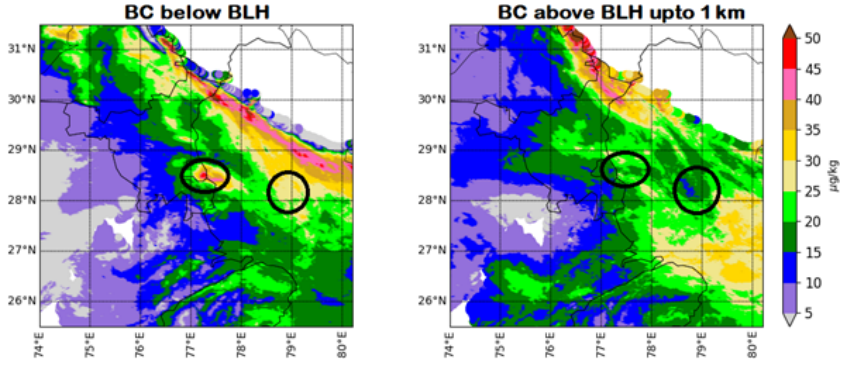


Figure A5. Simulated mass mixing ratio of black carbon integrated (left) up to boundary layer height and (right) above boundary layer height up to 1000 m. Regions marked by ovals indicate some regions where BC below BLH is significantly higher than BC above BLH. These regions exhibit a decrease in fog height with the *ARII-A* experiment, which can be seen in Fig. 10.

Code and data availability. Due to intellectual property right restrictions, the Met Office Unified Model is available for use under license for NCMRWF, being a core partner. For further information on how to apply for a license, see https://www.metoffice.gov.uk/research/approach/modelling-systems/unified-model (last access: 5 November 2026). The data used to initialize the DM-Chem1.0 are from METUM data which is cited in Jayakumar et al. (2021). The MODIS LWP and SSA datasets were acquired from the Level 1 and Atmosphere Archive and Distribution System (LAADS) Distributed Active Archive Center (DAAC) available at https://ladsweb.modaps.eosdis.nasa.gov (last access: 1 October 2025).

Author contributions. TJA and SB conceptualised the study, designed the experiments, and analyzed the results. SB performed the simulations and wrote the manuscript draft under the supervision of TJA. AJ, HG, AnJ, SM, and VSP proposed scientific suggestions and reviewed and edited the manuscript.

Competing interests. The contact author has declared that none of the authors has any competing interests.

Disclaimer. Publisher's note: Copernicus Publications remains neutral with regard to jurisdictional claims made in the text, published maps, institutional affiliations, or any other geographical representation in this paper. The authors bear the ultimate responsibility for providing appropriate place names. Views expressed in the text are those of the authors and do not necessarily reflect the views of the publisher.

Acknowledgements. This study was carried out within the framework of the "Weather and Climate Science for Service Partnership India" (WCSSP)–India, a collaborative initiative between the Ministry of Earth Sciences (MoES), Government of India and the Met Office, United Kingdom.

We thank these Principal Investigators for their efforts in establishing and maintaining the AERONET sites whose data were used in this study: Prof. Panuganti C. S. Devara (Amity University, Gurgaon), Dr. Amrit Kumar (Amity University, Gurgaon), Prof. Ramesh P. Singh (Kanpur), Prof. S. N. Tripathi (Kanpur), Dr. Pawan Gupta (Kanpur and Gandhi College, Ballia), and Dr. Elena Lind (Kanpur and Gandhi College, Ballia).

We also sincerely thank the anonymous reviewers for their constructive comments and suggestions, which substantially improved the quality and clarity of the manuscript.

Review statement. This paper was edited by Xiaohong Liu and reviewed by two anonymous referees.

References

Abdullah, B. H., Singh, P., Vaishya, A., Prasad, P., Rastogi, S., Gogoi, M. M., and Babu, S. S.: Decadal analysis of black carbon aerosols over the central Indo-Gangetic Plain: trends, source regions, and policy impact, Atmos. Res., 326, 108271, https://doi.org/10.1016/j.atmosres.2025.108271, 2025.

Ali, M. and Kumar, N.: Pulses in Indo-Gangetic Plains Status and strategies for area expansion and productivity gain, Indian Farming, 66, https://epubs.icar.org.in/index.php/IndFarm/article/view/72565 (last access: 5 November 2026), 2016.

Anurose, T. J., Jayakumar, A., Sandhya, M., Gordon, H., Aryasree, S., Mohandas, S., Bhati, S., and Prasad, V. S.: Unraveling the Mechanism of the Holes in the Blanket of Fog Over the Indo-Gangetic Plains: Are They Driven by Urban Heat Islands or Aerosol?, Geophys. Res. Lett., 51, e2023GL107252, https://doi.org/10.1029/2023GL107252, 2024.

Arun, N., Sarangi, C., and Qian, Y.: Particulate Pollution Increases Fog Duration Over the Indo-Gangetic Plain, Geophys. Res. Lett., 52, e2024GL114095, https://doi.org/10.1029/2024GL114095, 2025.

Bharali, C., Barth, M., Kumar, R., Ghude, S. D., Sinha, V., and Sinha, B.: Role of atmospheric aerosols in severe winter fog over the Indo-Gangetic Plain of India: a case study, Atmos. Chem. Phys., 24, 6635–6662, https://doi.org/10.5194/acp-24-6635-2024, 2024.

Boutle, I., Price, J., Kudzotsa, I., Kokkola, H., and Romakkaniemi, S.: Aerosol–fog interaction and the transition to well-mixed radiation fog, Atmos. Chem. Phys., 18, 7827–7840, https://doi.org/10.5194/acp-18-7827-2018, 2018.

Choudhary, V., Mandariya, A. K., Zhao, R., and Gupta, T.: Field evidence of brown carbon absorption enhancement linked to organic nitrogen formation in Indo-Gangetic Plain, Sci. Total Environ., 930, 172506, https://doi.org/10.1016/j.scitotenv.2024.172506, 2024.

Das, S. K., Jayaraman, A., and Misra, A.: Fog-induced variations in aerosol optical and physical properties over the Indo-Gangetic Basin and impact to aerosol radiative forcing, Ann. Geophys., 26, 1345–1354, https://doi.org/10.5194/angeo-26-1345-2008, 2008.

Deshpande, P., Meena, D., Tripathi, S., Bhattacharya, A., and Verma, M. K.: Event-based fog climatology and typology for cities in Indo-Gangetic plains, Urban Climate, 51, 101642, https://doi.org/10.1016/j.uclim.2023.101642, 2023.

Devi, N. L., Kumar, A., and Yadav, I. C.: PM10 and PM2.5 in Indo-Gangetic Plain (IGP) of India: Chemical characterization, source analysis, and transport pathways, Urban Climate, 33, 100663, https://doi.org/10.1016/j.uclim.2020.100663, 2020.

Ding, Q., Sun, J., Huang, X., Ding, A., Zou, J., Yang, X., and Fu, C.: Impacts of black carbon on the formation of advection–radiation fog during a haze pollution episode in eastern China, Atmos. Chem. Phys., 19, 7759–7774, https://doi.org/10.5194/acp-19-7759-2019, 2019.

Field, P. R., Hill, A., Shipway, B., Furtado, K., Wilkinson, J., Miltenberger, A., Gordon, H., Grosvenor, D. P., Stevens, R., and Van Weverberg, K.: Implementation of a double moment cloud microphysics scheme in the UK met office regional numerical weather prediction model, Q. J. Roy. Meteor. Soc., 149, 703–739, https://doi.org/10.1002/qj.4414, 2023.

Gautam, R. and Singh, M. K.: Urban Heat Island Over Delhi Punches Holes in Widespread Fog in the Indo-Gangetic Plains, Geophys. Res. Lett., 45, 1114–1121, https://doi.org/10.1002/2017GL076794, 2018.

Gautam, R., Hsu, N. C., Kafatos, M., and Tsay, S.: Influences of winter haze on fog/low cloud over the Indo-

Gangetic plains, J. Geophys. Res.-Atmos., 112, 2005JD007036, https://doi.org/10.1029/2005JD007036, 2007.

Ghosh, P., Boutle, I., Field, P., Hill, A., Jones, A., Mazoyer, M., Evans, K. J., Mahajan, S., Kang, H.-G., Xu, M., Zhang, W., Asch, N., and Gordon, H.: High sensitivity of simulated fog properties to parameterized aerosol activation in case studies from ParisFog, Atmos. Chem. Phys., 25, 11129–11156, https://doi.org/10.5194/acp-25-11129-2025, 2025.

Ghude, S. D., Bhat, G. S., Prabhakaran, T., Jenamani, R. K., Chate, D. M., Safai, P. D., Karipot, A. K., Konwar, M., Pithani, P., Sinha, V., Rao, P. S. P., Dixit, S. A., Tiwari, S., Todekar, K., Varpe, S., Srivastava, A. K., Bisht, D. S., Murugavel, P., Ali, K., Mina, U., Dharua, M., Rao, Y. J., Padmakumari, B., Hazra, A., Nigam, N., Shende, U., Lal, D. M., Chandra, B. P., Mishra, A. K., Kumar, A., Hakkim, H., Pawar, H., Acharja, P., Kulkarni, R., Subharthi, C., Balaji, B., Varghese, M., Bera, S., and Rajeevan, M.: Winter fog experiment over the Indo-Gangetic plains of India, Curr. Sci., 112, 767–784, 2017.

Ghude, S. D., Jenamani, R. K., Kulkarni, R., Wagh, S., Dhangar, N. G., Parde, A. N., Acharja, P., Lonkar, P., Govardhan, G., Yadav, P., Vispute, A., Debnath, S., Lal, D. M., Bisht, D. S., Jena, C., Pawar, P. V., Dhankhar, S. S., Sinha, V., Chate, D. M., Safai, P. D., Nigam, N., Konwar, M., Hazra, A., Dharmaraj, T., Gopalkrishnan, V., Padmakumari, B., Gultepe, I., Biswas, M., Karipot, A. K., Prabhakaran, T., Nanjundiah, R. S., and Rajeevan, M.: WiFEX: Walk into the Warm Fog over Indo-Gangetic Plain Region, B. Am. Meteorol. Soc., 104, E980–E1005, https://doi.org/10.1175/BAMS-D-21-0197.1, 2023.

Gordon, H., Field, P. R., Abel, S. J., Dalvi, M., Grosvenor, D. P., Hill, A. A., Johnson, B. T., Miltenberger, A. K., Yoshioka, M., and Carslaw, K. S.: Large simulated radiative effects of smoke in the south-east Atlantic, Atmos. Chem. Phys., 18, 15261–15289, https://doi.org/10.5194/acp-18-15261-2018, 2018.

Gordon, H., Carslaw, K. S., Hill, A. A., Field, P. R., Abraham, N. L., Beyersdorf, A., Corr-Limoges, C., Ghosh, P., Hemmings, J., Jones, A. C., Sanchez, C., Wang, X., and Wilkinson, J.: NUMAC: Description of the Nested Unified Model With Aerosols and Chemistry, and Evaluation With KORUS-AQ Data, J. Adv. Model. Earth Sy., 15, e2022MS003457, https://doi.org/10.1029/2022MS003457, 2023.

Holben, B. N., Eck, T. F., Slutsker, I., Tanré, D., Buis, J. P., Setzer, A., Vermote, E., Reagan, J. A., Kaufman, Y. J., Nakajima, T., Lavenu, F., Jankowiak, I., and Smirnov, A.: AERONET – A Federated Instrument Network and Data Archive for Aerosol Characterization, Remote Sens. Environ., 66, 1–16, https://doi.org/10.1016/S0034-4257(98)00031-5, (data available at https://aeronet.gsfc.nasa.gov/, last access: 28 October 2025), 1998.

India Meteorological Department (IMD): Climate Summary for the month of January 2023, Climate Research and Services (CRS), Ministry of Earth Sciences, Government of India, https://internal.imd.gov.in/press_release/20230206_pr_2142.pdf (last access: 26 October 2024), 2023.

Intergovernmental Panel on Climate Change (IPCC): Climate Change 2013: The Physical Science Basis, Contribution of Working Group I to the Fifth Assessment Report of the Intergovernmental Panel on Climate Change, edited by: Stocker, T. F., Qin, D., Plattner, G.-K., Tignor, M., Allen, S. K., Boschung, J., Nauels, A., Xia, Y., Bex, V., and Midgley, P. M., Cambridge University Press, Cambridge, United Kingdom and New York, NY, USA, 1535 pp., https://doi.org/10.1017/CBO9781107415324, 2013.

Jayakumar, A., Rajagopal, E. N., Boutle, I. A., George, J. P., Mohandas, S., Webster, S., and Aditi, S.: An operational fog prediction system for Delhi using the 330 m Unified Model, Atmos. Sci. Lett., 19, e796, https://doi.org/10.1002/asl.796, 2018.

Jayakumar, A., Gordon, H., Francis, T., Hill, A. A., Mohandas, S., Sandeepan, B. S., Mitra, A. K., and Beig, G.: Delhi Model with Chemistry and aerosol framework (DM-Chem) for high-resolution fog forecasting, Q. J. Roy. Meteor. Soc., 147, 3957–3978, https://doi.org/10.1002/qj.4163, 2021.

Jayakumar, A., Anurose, T. J., Bhati, S., Hendry, M. A., Hayman, G., Gordon, H., Field, P., Mohandas, S., Rumbold, H., Yadav, P., Dhangar, N. G., Parde, A., Wagh, S., Ghude, S., Ross, A. N., Smith, D., Dorling, S., George, J. P., Prasad, V. S., and Ravichandran, M.: Development of an Integrated Modeling Framework for Visibility and Air Quality Forecasting in Delhi, B. Am. Meteorol. Soc., 106, E261–E274, https://doi.org/10.1175/BAMS-D-24-0194.1, 2025.

Jenamani, R.: Development of intensity based fog climatological information system (daily and hourly) at IGI airport, New Delhi for use in fog forecasting and aviation, Mausam, 63, 89–112, 2012.

Kulkarni, R., Jenamani, R. K., Pithani, P., Konwar, M., Nigam, N., and Ghude, S. D.: Loss to Aviation Economy Due to Winter Fog in New Delhi during the Winter of 2011–2016, Atmosphere, 10, https://doi.org/10.3390/atmos10040198, 2019.

Kutty, S. G., Dimri, A. P., and Gultepe, I.: Climatic trends in fog occurrence over the Indo-Gangetic plains, Int. J. Climatol., 40, 2048–2061, https://doi.org/10.1002/joc.6317, 2020.

Levy, R., Hsu, C., Sayer, A., Mattoo, S., and Lee, J.: MODIS Atmosphere L2 Aerosol Product, NASA MODIS Adaptive Processing System, Goddard Space Flight Center, USA, https://doi.org/10.5067/MODIS/MOD04_L2.006, 2015.

Levy, R. C., Remer, L. A., Kleidman, R. G., Mattoo, S., Ichoku, C., Kahn, R., and Eck, T. F.: Global evaluation of the Collection 5 MODIS dark-target aerosol products over land, Atmos. Chem. Phys., 10, 10399–10420, https://doi.org/10.5194/acp-10-10399-2010, 2010.

Li, J., Carlson, B. E., and Lacis, A. A.: Using single-scattering albedo spectral curvature to characterize East Asian aerosol mixtures, J. Geophys. Res.-Atmos., 120, 2037–2052, https://doi.org/10.1002/2014JD022433, 2015.

Li, J., Carlson, B. E., Yung, Y. L., Lv, D., Hansen, J., Penner, J. E., Liao, H., Ramaswamy, V., Kahn, R. A., Zhang, P., Dubovik, O., Ding, A., Lacis, A. A., Zhang, L., and Dong, Y.: Scattering and absorbing aerosols in the climate system, Nature Reviews Earth & Environment, 3, 363–379, https://doi.org/10.1038/s43017-022-00296-7, 2022.

Li, X., Ma, Y., Wang, Y., Lu, S., Zhao, H., Liu, N., Hong, Y., and Wang, D: Characteristics of Turbulence and Aerosol Optical and Radiative Properties during Haze–Fog Episodes in Shenyang, Northeast China, Atmosphere, 12, https://doi.org/10.3390/atmos12121658, 2021.

Liu, L., Cheng, Y., Wang, S., Wei, C., Pöhlker, M. L., Pöhlker, C., Artaxo, P., Shrivastava, M., Andreae, M. O., Pöschl, U., and Su, H.: Impact of biomass burning aerosols on radiation, clouds, and precipitation over the Amazon: relative importance of aerosol–cloud and aerosol–radiation interactions, Atmos. Chem. Phys.,

20, 13283–13301, https://doi.org/10.5194/acp-20-13283-2020, 2020.

Liu, M., Shi, H., Song, J., and Fu, D.: Quantitation of the Surface Shortwave and Longwave Radiative Effect of Dust with an Integrated System: A Case Study at Xianghe, Sensors, 24, https://doi.org/10.3390/s24020397, 2024.

Maalick, Z., Kühn, T., Korhonen, H., Kokkola, H., Laaksonen, A., and Romakkaniemi, S.: Effect of aerosol concentration and absorbing aerosol on the radiation fog life cycle, Atmos. Environ., 133, 26–33, https://doi.org/10.1016/j.atmosenv.2016.03.018, 2016.

Mann, G. W., Carslaw, K. S., Spracklen, D. V., Ridley, D. A., Manktelow, P. T., Chipperfield, M. P., Pickering, S. J., and Johnson, C. E.: Description and evaluation of GLOMAP-mode: a modal global aerosol microphysics model for the UKCA composition-climate model, Geosci. Model Dev., 3, 519–551, https://doi.org/10.5194/gmd-3-519-2010, 2010.

Maronga, B. and Bosveld, F. C.: Key parameters for the life cycle of nocturnal radiation fog: a comprehensive large-eddy simulation study, Q. J. Roy. Meteor. Soc., 143, 2463–2480, https://doi.org/10.1002/qj.3100, 2017.

Mazoyer, M., Burnet, F., and Denjean, C.: Experimental study on the evolution of droplet size distribution during the fog life cycle, Atmos. Chem. Phys., 22, 11305–11321, https://doi.org/10.5194/acp-22-11305-2022, 2022.

Mehrotra, B. J., Srivastava, A. K., Singh, A., Parashar, D., Majumder, N., Singh, R. S., Choudhary, A., and Srivastava, M. K.: Long-Term Trend in Black Carbon Mass Concentration Over Central Indo-Gangetic Plain Location: Understanding the Implied Change in Radiative Forcing, J. Geophys. Res.-Atmos., 129, e2024JD040754, https://doi.org/10.1029/2024JD040754, 2024.

Mohandas, S., Jayakumar, A., Field, P. R., Anurose, T. J., Van Weverberg, K., Wilkinson, J. M., Indira Rani, S., Mamgain, A., Raphel, R., Apsara, K. S., Mitra, A. K., and Prasad, V. S.: Impact of cloud microphysical factors on the track prediction of recurved tropical cyclone Vayu (2019) in a convective-scale model, Q. J. Roy. Meteor. Soc., 151, e5047, https://doi.org/10.1002/qj.5047, 2025.

Mulcahy, J. P., Johnson, C., Jones, C. G., Povey, A. C., Scott, C. E., Sellar, A., Turnock, S. T., Woodhouse, M. T., Abraham, N. L., Andrews, M. B., Bellouin, N., Browse, J., Carslaw, K. S., Dalvi, M., Folberth, G. A., Glover, M., Grosvenor, D. P., Hardacre, C., Hill, R., Johnson, B., Jones, A., Kipling, Z., Mann, G., Mollard, J., O'Connor, F. M., Palmiéri, J., Reddington, C., Rumbold, S. T., Richardson, M., Schutgens, N. A. J., Stier, P., Stringer, M., Tang, Y., Walton, J., Woodward, S., and Yool, A.: Description and evaluation of aerosol in UKESM1 and HadGEM3-GC3.1 CMIP6 historical simulations, Geosci. Model Dev., 13, 6383–6423, https://doi.org/10.5194/gmd-13-6383-2020, 2020.

Navinya, C., Kapoor, T. S., Venkataraman, C., Phuleria, H. C., and Chakrabarty, R. K.: Brown Carbon Light Absorption over India: Research Status and Need for Discerning Climate Impacts, ACS EST Air, 2, 1115–1135, https://doi.org/10.1021/acsestair.5c00010, 2025.

Ojha, N., Sharma, A., Kumar, M., Girach, I., Ansari, T. U., Sharma, S. K., Singh, N., Pozzer, A., and Gunthe, S. S.: On the widespread enhancement in fine particulate matter across the Indo-Gangetic Plain towards winter, Sci. Rep., 10, 5862, https://doi.org/10.1038/s41598-020-62710-8, 2020.

Peng, Y., Wang, H., Zhang, X., Zheng, Y., Zhang, X., Zhang, W., Liu, Z., Gui, K., Liu, H., Wang, Y., and Che, H.: Aerosol-radiation interaction in the operational atmospheric chemistry model GRAPES_Meso5.1/CUACE and its impacts on mesoscale NWP in Beijing-Tianjin-Hebei, China, Atmos. Res., 280, 106402, https://doi.org/10.1016/j.atmosres.2022.106402, 2022.

Platnick, S., Ackerman, S., King, M., Wind, G., Meyer, K., Menzel, P., Frey, R., Holz, R., Baum, B., and Yang, P.: MODIS Atmosphere L2 Cloud Product (06_L2), NASA MODIS Adaptive Processing System, Goddard Space Flight Center, USA, https://doi.org/10.5067/MODIS/MOD06_L2.006, 2015.

Rai, A. K., Singh, A. K., Pati, J. K., Gupta, S., Chakarvorty, M., Niyogi, A., Pandey, A., Dwivedi, M. M., Pandey, K., and Prakash, K.: Assessment of topsoil contamination in an urbanized interfluve region of Indo-Gangetic Plains (IGP) using magnetic measurements and spectroscopic techniques, Environ. Monit. Assess., 191, 403, https://doi.org/10.1007/s10661-019-7525-x, 2019.

Ramachandran, S. and Rupakheti, M.: Trends in the types and absorption characteristics of ambient aerosols over the Indo-Gangetic Plain and North China Plain in last two decades, Sci. Total Environ., 831, 154867, https://doi.org/10.1016/j.scitotenv.2022.154867, 2022.

Ramachandran, S., Rupakheti, M., and Cherian, R.: Insights into recent aerosol trends over Asia from observations and CMIP6 simulations, Sci. Total Environ., 807, 150756, https://doi.org/10.1016/j.scitotenv.2021.150756, 2022.

Sarin, T. S. and Vinoj, V.: Assessing the relationship between atmospheric aerosols and maximum surface air temperature over the Indian region, Sci. Rep., 16, 9483, https://doi.org/10.1038/s41598-026-40641-0, 2026.

Sarkar, A. and Panda, J.: Significance of anthropogenic black carbon in modulating atmospheric and cloud properties through aerosol-radiation interaction during a winter-time fog-haze, Atmos. Environ., 334, 120720, https://doi.org/10.1016/j.atmosenv.2024.120720, 2024.

Shamjad, P. M., Tripathi, S. N., Pathak, R., Hallquist, M., Arola, A., and Bergin, M. H.: Contribution of Brown Carbon to Direct Radiative Forcing over the Indo-Gangetic Plain, Environ. Sci. Technol., 49, 10474–10481, https://doi.org/10.1021/acs.est.5b03368, 2015.

Shin, S.-K., Tesche, M., Noh, Y., and Müller, D.: Aerosol-type classification based on AERONET version 3 inversion products, Atmos. Meas. Tech., 12, 3789–3803, https://doi.org/10.5194/amt-12-3789-2019, 2019.

Singh, M. K. and Gautam, R.: Developing a long-term high-resolution winter fog climatology over south Asia using satellite observations from 2002 to 2020, Remote Sens. Environ., 279, 113128, https://doi.org/10.1016/j.rse.2022.113128, 2022.

Smith, D. K. E., Dorling, S. R., Renfrew, I. A., Ross, A. N., and Poku, C.: Fog trends in India: Relationships to fog type and western disturbances, Int. J. Climatol., 43, 818–836, https://doi.org/10.1002/joc.7832, 2023.

Smith, D. K. E., Reka, S., Dorling, S. R., Ross, A. N., Renfrew, I. A., Jayakumar, A., Anurose, T. J., Parde, A. N., Ghude, S. D., and Rumbold, H.: Forecasts of fog events in northern India dramatically improve when weather prediction models include ir-

rigation effects, Communications Earth & Environment, 5, 141, https://doi.org/10.1038/s43247-024-01314-w, 2024.

Srivastava, P., Pal, D. K., Aruche, K. M., Wani, S. P., and Sahrawat, K. L.: Soils of the Indo-Gangetic Plains: a pedogenic response to landscape stability, climatic variability and anthropogenic activity during the Holocene, Earth-Sci. Rev., 140, 54–71, https://doi.org/10.1016/j.earscirev.2014.10.010, 2015.

Su, T., Li, Z., Li, C., Li, J., Han, W., Shen, C., Tan, W., Wei, J., and Guo, J.: The significant impact of aerosol vertical structure on lower atmosphere stability and its critical role in aerosol–planetary boundary layer (PBL) interactions, Atmos. Chem. Phys., 20, 3713–3724, https://doi.org/10.5194/acp-20-3713-2020, 2020.

Theethai-Jacob, A., Jayakumar, A., Gupta, K., Mohandas, S., Hendry, M. A., Smith, D. K. E., Francis, T., Bhati, S., Parde, A. N., Mohan, M., Mitra, A. K., Kumar Gupta, P., Chauhan, P., Jenamani, R. K., and Ghude, S.: Implementation of the urban parameterization scheme in the Delhi model with an improved urban morphology, Q. J. Roy. Meteor. Soc., 149, 40–60, https://doi.org/10.1002/qj.4382, 2023.

Thomas, A., Sarangi, C., and Kanawade, V. P.: Recent Increase in Winter Hazy Days over Central India and the Arabian Sea, Sci. Rep., 9, 17406, https://doi.org/10.1038/s41598-019-53630-3, 2019.

Tilstra, L. G., Tuinder, O. N. E., and Stammes, P.: GOME-2 Absorbing Aerosol Index: Statistical analysis, comparison to GOME-1 and impact of instrument degradation, in: Proceedings of the 2010 EUMETSAT Meteorological Satellite Conference, Córdoba, Spain, EUMETSAT P.57, https://www-cdn.eumetsat.int/files/2020-04/pdf_conf_p57_s4_12_tilstra_p.pdf (last access: 5 November 2026), 2010.

van Weverberg, K., Morcrette, C. J., Boutle, I., Furtado, K., and Field, P. R.: A Bimodal Diagnostic Cloud Fraction Parameterization. Part I: Motivating Analysis and Scheme Description, Mon. Weather Rev., 149, 841–857, https://doi.org/10.1175/MWR-D-20-0224.1, 2021.

Wagh, S., Kulkarni, R., Lonkar, P., Parde, A. N., Dhangar, N. G., Govardhan, G., Sajjan, V., Debnath, S., Gultepe, I., Rajeevan, M., and Ghude, S. D.: Development of visibility equation based on fog microphysical observations and its verification using the WRF model, Model. Earth Syst. Environ., 9, 195–211, https://doi.org/10.1007/s40808-022-01492-6, 2023.

Wesely, M. L.: Parameterization of surface resistances to gaseous dry deposition in regional-scale numerical models, Atmos. Environ. (1967), 23, 1293–1304, https://doi.org/10.1016/0004-6981(89)90153-4, 1989.

Wilkinson, J. M., Porson, A. N. F., Bornemann, F. J., Weeks, M., Field, P. R., and Lock, A. P.: Improved microphysical parametrization of drizzle and fog for operational forecasting using the Met Office Unified Model, Q. J. Roy. Meteor. Soc., 139, 488–500, https://doi.org/10.1002/qj.1975, 2013.

World Population Review: Largest Cities by Population 2024, https://worldpopulationreview.com/cities, last access: 30 October 2024.

Wu, J., Bei, N., Hu, B., Liu, S., Wang, Y., Shen, Z., Li, X., Liu, L., Wang, R., Liu, Z., Cao, J., Tie, X., Molina, L. T., and Li, G.: Aerosol–photolysis interaction reduces particulate matter during wintertime haze events, P. Natl. Acad. Sci. USA, 117, 9755–9761, https://doi.org/10.1073/pnas.1916775117, 2020.

Yan, S., Zhu, B., Zhu, T., Shi, C., Liu, D., Kang, H., Lu, W., and Lu, C.: The Effect of Aerosols on Fog Lifetime: Observational Evidence and Model Simulations, Geophys. Res. Lett., 48, e2020GL61803, https://doi.org/10.1029/2020GL091156, 2021.

Yang, H., Chen, L., Liao, H., Zhu, J., Wang, W., and Li, X.: Weakened aerosol–radiation interaction exacerbating ozone pollution in eastern China since China's clean air actions, Atmos. Chem. Phys., 24, 4001–4015, https://doi.org/10.5194/acp-24-4001-2024, 2024.